

Discovery of 2-Phenylamino-imidazo[4,5-*h*]isoquinolin-9-ones: A New Class of Inhibitors of Lck Kinase

Roger J. Snow,^{*,†,‡} Mario G. Cardozo,^{†,‡} Tina M. Morwick,^{†,‡} Carl A. Busacca,[§] Yong Dong,[§] Robert J. Eckner,^{||} Stephen Jacober,[†] Scott Jakes,^{||} Suresh Kapadia,[§] Susan Lukas,^{||} Maret Panzenbeck,[⊥] Gregory W. Peet,^{||} Jeffrey D. Peterson,[⊥] Anthony S. Prokopowicz, III,[†] Rosemarie Sellati,[⊥] Robert M. Tolbert,[#] Matt A. Tschantz,[†] and Neil Moss[†]

Departments of Medicinal Chemistry, Chemical Development, Biology, Pharmacology, and Information Technology, Boehringer Ingelheim Pharmaceuticals Inc., 900 Ridgebury Road, Ridgefield, Connecticut 06877

Received March 11, 2002

An imidazo[4,5-*h*]isoquinolin-7,9-dione (**1**) was identified as an adenosine 5'-triphosphate competitive inhibitor of lck by high throughput screening. Initial structure–activity relationship studies identified the dichlorophenyl ring and the imide NH as important pharmacophores. A binding model was constructed to understand how **1** binds to a related kinase, hck. These results suggested that removing the *gem*-dimethyl group and flattening the ring would enhance activity. This was realized by converting **1** to the imidazo[4,5-*h*]isoquinolin-9-one (**20**), resulting in an 18-fold improvement in potency against lck and a 50-fold increase in potency in a cellular assay.

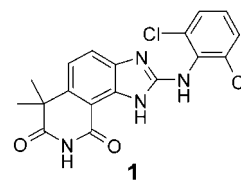
Introduction

The tyrosine kinase p56^{lck} (lck) is present in T cells and is known to be required to initiate the activation response from the T cell receptor (TCR) intracellular domain to other signaling proteins.¹ T cells that lack lck are unable to respond to stimulation through the TCR.^{2,3} Transfection of lck back into these cell lines restores TCR responsiveness. Similarly, the T cell response is abolished by transfection of a dominant negative form of lck.⁴ Inactivation of the lck gene in mice results in impairment of thymocyte development.⁵ These lck (-/-) mice have a complete lack of CD4+ cells and are unable to mount antigen-dependent immune responses. The conclusion drawn from these studies is that lck plays a crucial role in T cell maturation and antigen-induced T cell activation. Therefore, an inhibitor of lck should effectively block T cell function, act as an immunosuppressive agent, and have potential therapeutic utility in treating autoimmune diseases.⁶

There have been several reports of inhibitors of lck kinase. Much of the earlier work was on natural products including lavendustin A,⁷ piceatannol⁸ and damnacanthal,⁹ and compounds derived from them, as well as flavones¹⁰ related to the nonselective tyrosine kinase inhibitor quercetin. Other inhibitors have been derived from the tyrphostins.¹¹ Subsequently, Myers¹² reported a series of quinazolines with lck activity, and Hanke et al.¹³ disclosed the pyrazolopyrimidine PP1, which has selectivity for the src family of kinases, including lck. A related series of compounds have recently been disclosed by the BASF group.^{14,15} Kraker et al.¹⁶ have reported on pyrido[2,3-*d*]pyridine kinase inhibitors, which have potent activity against lck.

Inhibitors of the src family¹⁷ and other kinases have recently been reviewed.¹⁸ We now report the results of our initial studies on inhibitors of lck, which have led to a new structural class of kinase inhibitor.

We embarked on a program to find novel inhibitors of lck that are potent in cellular assays and have in vivo activity. A screening program was initiated that identified the imidazo[4,5-*h*]isoquinoline-7,9-dione (**1**) as a hit structure. This compound was shown to be an adenosine 5'-triphosphate (ATP) competitive inhibitor of lck, with IC₅₀ = 0.46 μM in a lck kinase assay. Compound **1** was active in a T cell assay of anti-CD3-induced calcium influx, EC₅₀ = 9.7 μM. We carried out structure–activity relationship (SAR) studies on **1**, which identified the essential elements of the pharmacophore. A binding model was developed to understand how this compound interacts with the enzyme. This information was used to develop a new structural class of lck inhibitors with greatly improved activity.



Chemistry

The general route to compound **1** is shown in Scheme 1. Alkylation of dinitrile **2** proceeded well under phase transfer conditions, to give the geminally dialkylated product. Sequential reaction with two different alkyl halides was achieved in one pot to give **3c**. As reported,¹⁹ cyclization to the homophthalimide occurred on treatment with 90% H₂SO₄ for the dimethyl compound **3a**. With larger substituents, the major product isolated was the anhydride **4b,c**, as indicated by IR and the lack of an NH in the nuclear magnetic resonance (NMR) spectrum. The anhydrides were stable to aqueous workup and chromatography and were converted to the

* To whom correspondence should be addressed. Tel: 203-798-4060. Fax: 203-791-6072. E-mail: rsnow@rdg.boehringer-ingelheim.com.

[†] Department of Medicinal Chemistry.

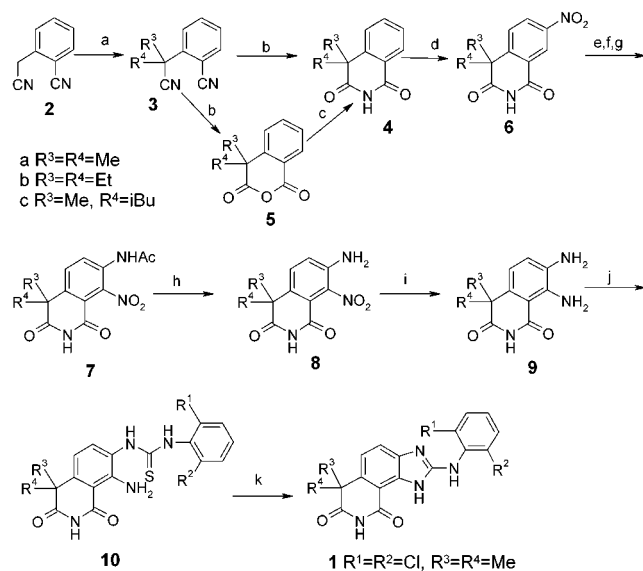
[‡] These authors contributed equally to this work.

[§] Department of Chemical Development.

^{||} Department of Biology.

[⊥] Department of Pharmacology.

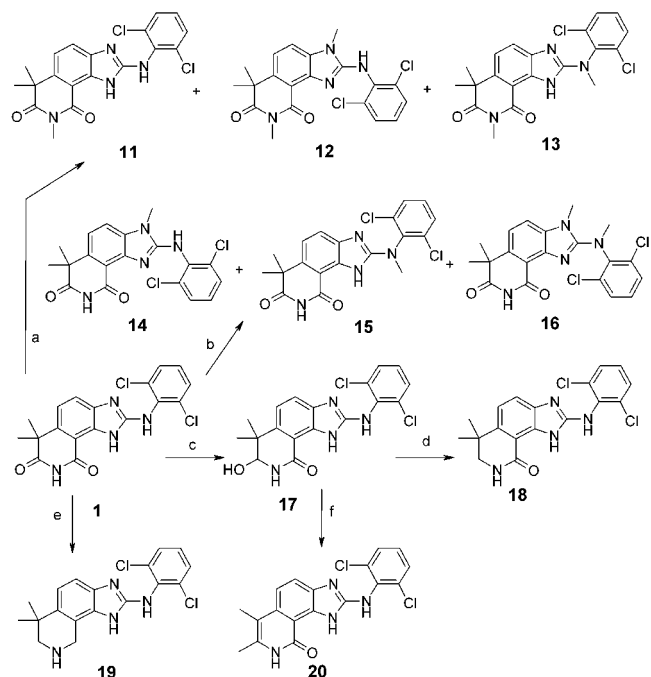
[#] Department of Information Technology.

Scheme 1. Synthesis of Imidazo[4,5-h]isoquinoline-7,9-diones^a


^a Reagents: (a) R³I, R⁴I, Bu₃NBnBr, NaOH; (b) 90% H₂SO₄, room temperature; (c) NH₄OH, THF, 65 °C; (d) HNO₃, H₂SO₄, 0 °C; (e) H₂, Pd/C, MeOH; (f) Ac₂O; (g) 90% HNO₃, -20 °C; (h) 90% H₂SO₄, 60 °C; (i) H₂, PtO₂, MeOH; (j) ArNCS, EtOAc, room temperature; (k) DCC, THF, reflux.

imides **3b,c** by heating with ammonium hydroxide in tetrahydrofuran (THF). The nitrogens of the benzimidazole were introduced in a known²⁰ four step sequence of nitration at C7, reduction, acetylation, and a second nitration at C8 to give **7**. Removal of the acetyl group was best achieved by brief treatment with concentrated H₂SO₄. Hydrogenation of **8** yielded the diamine **9**, which was reacted with substituted phenyl isothiocyanates to give the corresponding thiourea **10**, and cyclized to the benzimidazole **1** by treatment with DCC. Analogues of **1** were obtained from **9** by the same method. Thiourea formation worked well for isothiocyanates with electron-withdrawing groups but was slow when bulky or electron-donating substituents were present. This approach was limited to compounds that were geminally substituted in the homophthalimide ring. Attempts to carry out the sequence on mono- or unsubstituted homophthalimides were unsuccessful because of oxidation of the benzylic position during the nitration step. To investigate the effect of removing the methyl groups from **1**, alternative approaches were needed, as discussed below.

Scheme 2 summarizes reactions carried out on **1**. Methylation in the presence of base occurs first on the imide nitrogen, to give **11**, accompanied by two dimethylated products, **12** and **13**. The structure of **12** was confirmed by X-ray crystallography (Figure 1), showing the methyl groups on the imide and benzimidazole N3 nitrogens. In the crystal, the dichlorophenyl ring adopts a conformation away from the methyl group (see below). When **1** was treated with methyl iodide without base, alkylation on the imide did not occur, and a mixture of two monomethyl derivatives **14** and **15** was obtained, resulting from alkylation on one ring nitrogen and the exocyclic nitrogen, respectively, along with the dimethyl derivative **16**. The site of methylation in **14** and **15** was determined by a combination of two-dimensional (2D) NMR experiments including HMBC (heteronuclear

Scheme 2. Reactions of Compound **1**^a


^a Reagents: (a) NaHMDS, MeI, THF; (b) MeI, THF; (c) NaBH₄, THF, H₂O; (d) NaBH₄, TFA; (e) LiAlH₄, THF; (f) H₂SO₄, room temperature.

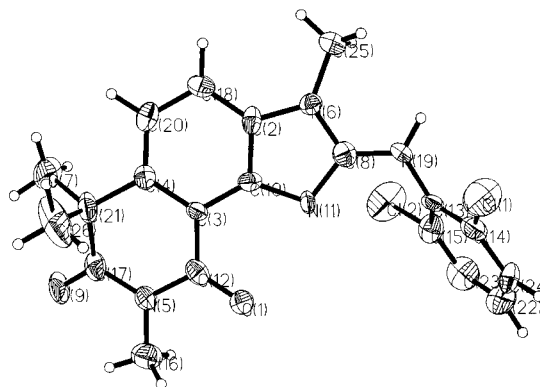
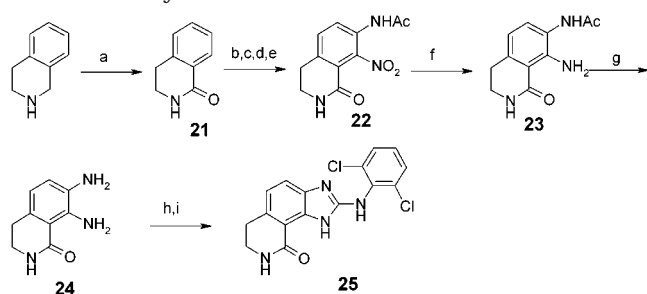


Figure 1. X-ray structure of **12** shown in ORTEP representation. Thermal ellipsoids are drawn at 80% probability.

multiple bond correlation spectroscopy), HMQC (heteronuclear multiple quantum correlation spectroscopy), and NOESY (nuclear Overhauser effect spectroscopy). No alkylation was observed at the ring nitrogen (N1) adjacent to the carbonyl, presumably due to steric hindrance. Initial reduction of the imide with NaBH₄ in wet THF took place selectively at the carbonyl adjacent to the *gem*-dimethyl group to give the labile hydroxylactam **17**, which was characterized by NMR including HMBC. Precedence for the regiochemistry of reduction of cyclic imides at the apparently more hindered site has been described.²¹ One explanation involves the methyl groups blocking the trajectory of nucleophilic addition to the opposite carbonyl group. Further reduction of **17** with excess NaBH₄ in the presence of trifluoroacetic acid (TFA) produced the lactam **18**, as well as the piperidine **19**. Alternatively, if the reducing agent NaBH(O₂CCF₃)₃ was generated in situ prior to addition of the hydroxy lactam substrate, **18** became the exclusive product. With **17** in hand, we recognized an opportunity to explore compounds lacking

Scheme 3. Synthesis of Lactam **25**^a

^a Reagents: (a) PhIO, NaOH; (b) HNO₃, H₂SO₄, 0 °C; (c) H₂, Pd/C, MeOH; (d) Ac₂O, Et₃N; (e) 90% HNO₃, -20 °C; (f) Fe, HCl, EtOH; (g) N₂H₄·H₂O, 90 °C; (h) ArNCS, EtOAc, room temperature; (i) DCC, THF, reflux.

the geminal substitution in the homophthalimide ring of **1**, which was particularly exciting in view of the molecular modeling results (see below). Accordingly, **17**, on treatment with sulfuric acid, underwent a Wagner–Meerwein rearrangement²² to yield the imidazo[4,5-*h*]isoquinolin-9-one **20**, in good yield.

An alternative approach to compounds lacking the *gem*-dimethyl substitution was explored with **25**, the unsubstituted analogue of lactam **18** (Scheme 3). This was prepared from dihydroisoquinolinone **21**, obtained by oxidation of tetrahydroisoquinoline with iodosyl benzene,²³ in an analogous manner to the synthesis of **1**, again using two successive nitrations to produce **22**. Deprotection of the acetamide proved much more troublesome than in the imide series. Treatment of **22** under acidic, or basic conditions, which were successful for the deprotection of **7**, led to ring opening of the lactam. Reduction of the nitro group to **23** decreased the electrophilicity of the lactam carbonyl and suppressed ring opening, though closure of the acetamide to a 2-methyl benzimidazole was observed as a side reaction. After some experimentation, heating with hydrazine was found to be effective in forming the diamine in modest yield, which was converted directly to the thiourea **24** before purification and then cyclized to **25** as before.

Initial SAR. Compounds were assayed in an in vitro assay using recombinant human lck kinase catalytic domain with polyGluTyr (4:1) as substrate (Table 1). In this assay, **1** had an IC₅₀ of 0.46 μM. Initial studies were aimed at exploring the SAR of **1** to identify important pharmacophores and sites to improve activity. Modification of the dichlorophenyl ring of **1** showed the importance of the 2,6-disubstitution pattern. Compounds **26** and **27**, with just one ortho chlorine, showed a significant decrease in activity. From the high throughput screen, it was known that the unsubstituted phenyl analogue was inactive, as was the compound in which the phenyl ring was replaced by a methyl group (data not shown). The chlorines could be replaced by methyl without loss of activity (**29** and **30**), but smaller groups such as F (**31**) and particularly larger ethyl groups (**32**) at two and six decreased potency. Substitution with chlorine at C4 was tolerated, but the tetrachloro derivative **35** was inactive. In the imide ring, it was found that methylation of the nitrogen **11** considerably reduced activity, but removal of one carbonyl to give the lactam **18** retained most of the activity of **1**. Removal of the

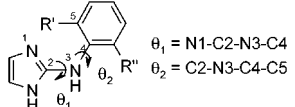
Table 1. Enzyme Inhibition and Cellular Data

no.	ring	R	R ³	R ⁴	X	IC ₅₀ (μM) ^a	EC ₅₀ (μM) ^b
1	A	2,6-Cl ₂	Me	Me	NH	0.46	9.7 ± 0.7
26	A	2-Cl	Me	Me	NH	>40	NT
27	A	2,4-Cl ₂	Me	Me	NH	>40	NT
28	A	4-Cl	Me	Me	NH	>40	NT
29	A	2-Cl,6-Me	Me	Me	NH	0.77	2.9 ± 0.9
30	A	2,6-Me ₂	Me	Me	NH	0.46	4.6 ± 0.8
31	A	2,6-F ₂	Me	Me	NH	11	NT
32	A	2,6-Et ₂	Me	Me	NH	>40	NT
33	A	2,4,6-Cl ₃	Me	Me	NH	0.73	4.3 ± 0.8
34	A	2,4,6-Br ₃	Me	Me	NH	0.6	7.3 ± 1.4
35	A	2,3,5,6-Cl ₄	Me	Me	NH	>40	NT
36	A	2,6-Cl ₂	Me	Me	CH ₂	9.6	NT
15	A	2,6-Cl ₂	Me	Me	NMe	2.5	NT
14	c	2,6-Cl ₂	Me	Me	NH	2.5	NT
11	c	2,6-Cl ₂	Me	Me	NH	9.6	NT
37	A	2,6-Cl ₂	Et	Et	NH	5.9	NT
38	A	2,6-Cl ₂	Me	^t Bu	NH	5.1	NT
18	C	2,6-Cl ₂	Me	Me	NH	1.1	5.2 ± 0.9
25	C	2,6-Cl ₂	H	H	NH	0.38	1.8 ± 0.5
19	D	2,6-Cl ₂	Me	Me	NH	>40	NT
20	B	2,6-Cl ₂				0.026	0.19 ± 0.01
39	B	2-Cl				0.15	NT
40	B	2-Cl,6-Me				0.027	0.34 ± 0.1
41	B	2,4,6-Cl ₃				0.018	0.42 ± 0.05
42	B	2,4,6-Br ₃				0.025	0.61 ± 0.03

^a IC₅₀ values for inhibition of lck. For active compounds, these are means of two or more separate determinations, in duplicate. Variation was generally within ±30% of the mean. ^b EC₅₀ values for inhibition of Ca release in Jurkat cells. Values are the means of two or more separate experiments in duplicate ± SD. ^c See Scheme 2 for structure; NT means not tested.

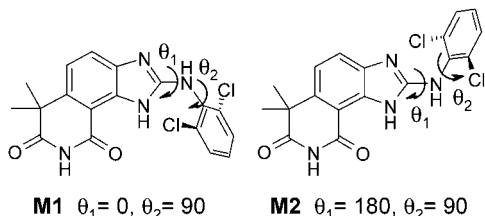
second carbonyl, however, resulted in an inactive piperidine analogue. These results suggested that the imide might be involved in a hydrogen-bonding interaction. Modification of the *gem*-dimethyl group of **1**, to increase the size of either one (**38**), or both, methyl groups (**37**) again reduced activity about 10-fold. At this point in our SAR studies, we had a clear picture of the important features of the molecule, but none of the changes had led to any improvement in potency. To understand how the molecule interacts with lck and to find ways to enhance binding, we constructed a computer model of the binding site.

Inhibitor Binding Model. At the time this work was initiated, there was little structural information available for lck. However, the three-dimensional (3D) structure of two homologous src family kinases, c-src²⁴ and hck,²⁵ were known, both of which have a high degree of identity with lck in the adenine binding site. Of the 16 residues that line the ATP site, only one, which is on the periphery of the binding site, differs between hck, src, and lck. Phe340 in hck is Tyr in lck and src, but the remaining 14 residues are identical in all three enzymes. We chose hck as a surrogate for lck in our studies since this had been crystallized in complexes with quercetin and with the ATP analogue, ADPNP, whereas the c-src structure was determined as the free enzyme. The initial SAR studies identified key pharmacophores. The first step in building the

Table 2. Conformational Search on Phenylamino Imidazoles


R'	R''	θ_1	θ_2	$\Delta\Delta E^a$	R'	R''	θ_1	θ_2	$\Delta\Delta E^a$
Cl	Cl	0	0, 180	5.8	H	H	0	0, 180	0.0
		0	90, 270	0.0			0	90, 270	0.9
		180	0, 180	5.5			180	0, 180	0.0
H	Cl	180	90, 270	0.0	H	Cl	180	90, 270	0.7
		0	0	0.0			180	0	6.1
		0	90, 270	0.7			180	90, 270	1.3
		0	180	15.0			180	180	0.0

^a Energy of each conformer after minimization, expressed in kcal/mol, relative to the global minimum for each compound.

**Figure 2.** Minimum energy conformations of **1**.

model was to define the preferred conformation of the inhibitor. The hydrophobic 2,6-dichlorophenyl moiety was clearly important. The role of this 2,6-disubstitution may be to stabilize the bound conformation of the inhibitor and/or to participate in a specific hydrophobic interaction with the protein. To evaluate the effect of the chlorine atoms on the conformation of the aniline moiety, we studied the conformational profile of the 2,6-dichloro, 2-chloro, and unsubstituted aniline attached to imidazole as a model of the tricyclic core of **1**, including the effect of solvation by water (Table 2). The conformational analysis around the N–Ph bond (θ_2) was performed at 30° increments. Both planar conformations of the amino imidazole bond ($\theta_1 = 0, 180^\circ$) were analyzed. In each case, the internal energies for the rotamers were computed with an ab initio quantum mechanics Hartree–Fock method using a 6-31G** basis set as implemented in Gaussian94.³⁷ The solvent contribution to the conformational energy was evaluated by computing the hydration free energy for each rotamer using a continuum solvation model.^{26,27} The apparent conformational energy in solution (ΔE_s) was obtained by adding the internal energy and hydration free energy contributions for each rotamer (Table 2). Analysis of the difference in ΔE_s ($\Delta\Delta E_s$) clearly indicates that the 2,6-disubstituted analogue is more stable at a 90° torsion angle (θ_2) relative to the imidazole ring. This is true for both conformations studied of θ_1 , corresponding to conformers M1 and M2 (Figure 2). The monochloro analogue is more stable in the two planar conformations with the Cl remote from the imidazole. However, the difference in energy for $\theta_2 = 90^\circ$ is only 0.7 and 1.3 kcal/mol, respectively. Finally, the unsubstituted analogue is also more stable in the planar conformations, but the energy at $\theta_2 = 90^\circ$ is only 0.9 and 0.7 kcal/mol, respectively. These results support the idea that the bound conformation of **1** has the phenyl ring inclined at 90° to the imidazole but also suggest that the lack of activity for the monosubstituted and unsubstituted analogues

is not entirely due to conformational differences. Both of these analogues can adopt the out-of-the-plane conformation at a low energy cost. Additional contribution to activity should be expected from a favorable hydrophobic effect.

The first step in deriving a model of the binding mode of **1** was to validate a docking procedure and to select a suitable force field. Thus, we used the grid-based program Autodock^{28,29} to perform docking experiments with quercetin, which had been cocrystallized with hck.²⁵ We found that the Amber force field,³⁰ with a 6–10 Lennard–Jones potential, gave the best results with a rms deviation of 0.25 Å as compared to the corresponding X-ray crystal structure. Electrostatic contributions were computed using Amber and ESP charges³¹ for the protein and ligand, respectively.

The importance of the dichlorophenyl moiety also provided insight into the binding mode for the series. The structures of all known src family kinases contain a clearly defined hydrophobic pocket, which is not occupied by ATP but is occupied by the substituted phenyl of quercetin in its complex with hck. We anticipated that the dichlorophenyl ring would occupy this pocket. The first docking attempts using **1** did not produce any ligand orientation with the dichlorophenyl moiety located inside the pocket. These docking experiments were performed for both conformations of the amino benzimidazole ($\theta_1 = 0, 180^\circ$), and free rotation around the aniline bond (θ_2). Additional docking experiments, allowing free rotation around θ_1 , yielded some orientations with the dichlorophenyl moiety inside the hydrophobic pocket. However, in all cases, θ_1 adopted torsion angles close to 90°, which twisted the benzimidazole core out of the plane occupied by ATP, which was clearly an energetically unfavorable conformation of the inhibitor. This conformation was also incompatible with hydrogen bonding to the hinge region, a feature found in all known kinase–inhibitor complexes. As noted, the initial SAR indicated that the imide nitrogen might act as a hydrogen bond donor, but none of the docking experiments using the whole molecule (**1**) produced any ligand orientation with hydrogen bond motifs in agreement with the SAR. This shortcoming could be the result of intrinsic protein flexibility and/or an induced fit upon ligand binding. These effects are not usually taken into account in conventional docking algorithms. If intrinsic protein flexibility is the issue, a typical approach is to evaluate possible protein dynamics, for example, by means of molecular simulations. In this case, to establish potential H bond interactions, we applied a molecular decomposition technique. This method has been used with success in several quantitative SAR studies³² and assumes that the ligand can be decomposed into moieties with apparent independent SAR and uncoupled conformational and electronic properties. The observed SAR, as well as the conformational studies, suggested that this could be the case in the current series. Therefore, new docking experiments were performed using the tricyclic core of **1**, with the dichlorophenyl replaced by a methyl group. Using this moiety as a hydrogen bond probe, we were able to identify various intermolecular hydrogen-bonding interactions. The most common patterns observed, which also gave high docking scores, showed a bidentate H

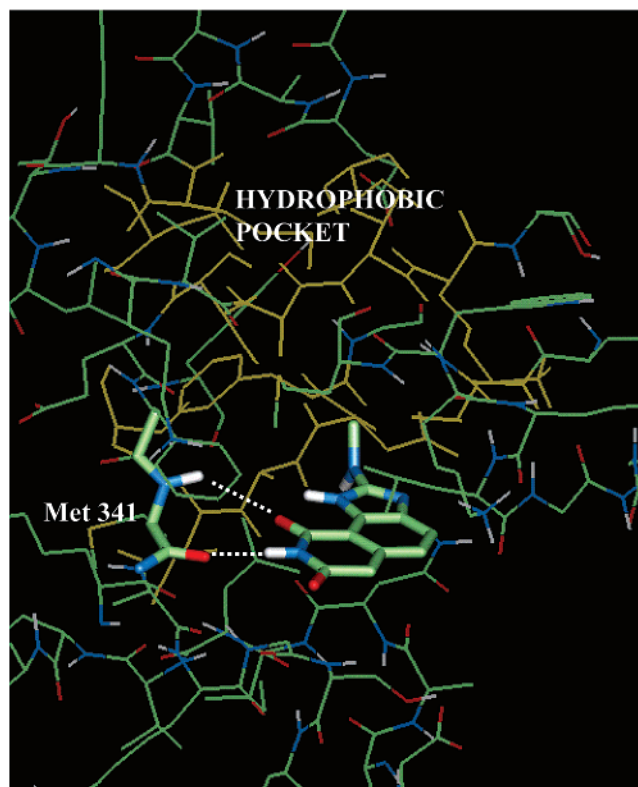


Figure 3. Binding mode of imidazoisoquinolindione to hck. The 2-amino-imidazoquinolindione core is docked into the ATP site of hck, showing two H bonds to Met341 in the hinge region (dashed lines), and the location of the hydrophobic pocket.

bond motif with the hinge region of the protein (Figure 3). This binding mode corresponds to one H bond between the C9 carbonyl oxygen of the ligand and the backbone NH of Met341 and a second H bond between the backbone CO of the same residue and the imide NH. This is an interaction that differs from that seen with ATP,²⁵ which forms two H bonds, to the NH of Met341 and the CO of Glu339, but is similar to the hydrogen-bonding pattern observed with certain inhibitors of CDK2³³ and FGFR kinase.³⁴

An important feature of this orientation is that the exocyclic amine is pointing toward the hydrophobic pocket. This proposed binding mode of the tricyclic core allowed us to build in the dichlorophenyl, so that it occupied the hydrophobic pocket, to generate a preliminary model for the binding of **1**. However, it was found that both possible low energy conformations of the exocyclic amine (Figure 2, $\theta_1 = 0$ or 180° , referred to as conformers M1 and M2, respectively) could be docked into the model, and initially, it was uncertain which of these was correct. Both conformations of **1** were refined using a combination of molecular dynamics (MD) simulations and energy minimization with an explicit solvent model. Details of the MD protocol and minimization are given in the Experimental Section. Figure 4 shows the difference in orientation of the hydrophobic moiety and a partial shift of the core relative to the hinge domain. Both conformations show the two hydrogen bonds between the imide and the hinge region described above. Two observations support M2 being the correct conformer. First, the model suggests the possibility for an additional hydrogen bond for this conformer between the exocyclic NH and the side chain oxygen of Thr338.

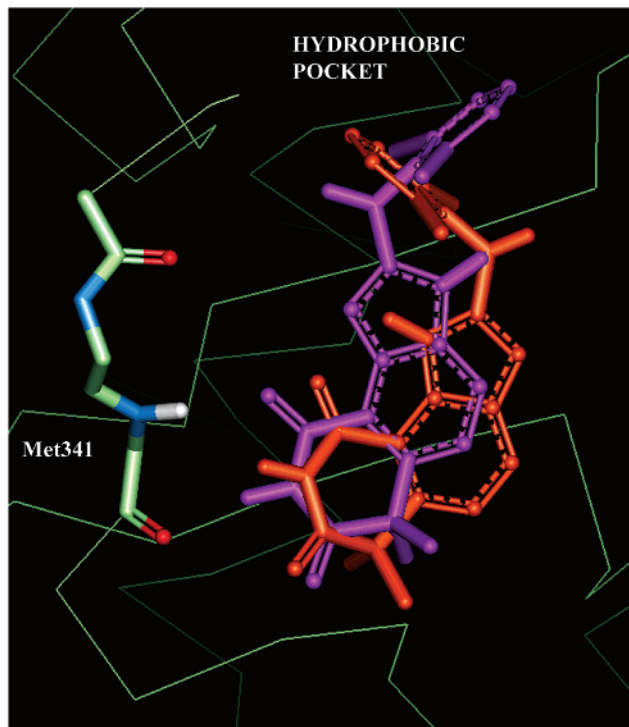


Figure 4. Docking of the two possible conformers of **1**, M1 (red) and M2 (magenta), into hck.

Some evidence for this additional interaction can be obtained from the SAR, since either methylation of the exocyclic NH to give **15** or replacement of the NH by CH_2 (**36**) causes a 5- and 20-fold decrease in activity, respectively. Second, methylation of N3 (**14**) is also detrimental. This compound would be expected to adopt the conformation corresponding to M1, due to steric interactions between the methyl and the phenyl ring. This conformation is seen in the X-ray structure of **12** (Figure 1), which also has a methyl group at N3. Because there appears to be room in the binding site to accommodate a methyl group at this position, this observation suggests that the methyl group in **14** forces the molecule to adopt an unfavorable conformation for binding. Neither **15** or **36** can form the third H bond, but the loss of activity could also be due to steric bulk of the *N*-methyl group in **15** or to conformational changes in **36**, resulting from replacing the sp^2 N with sp^3 C. However, conformational analysis of **36** indicated that the minimum energy conformation is equivalent to that of M2, with $\theta_1 = 180^\circ$ and $\theta_2 = 90^\circ$. This result suggested that the decreased potency of **36** is not due to the difference in the conformational profile but to the loss of an H bond to Thr338.

Although not conclusive, the balance of evidence favored M2 as the correct binding conformation, and all subsequent analysis focused on this orientation. A related binding model has been proposed by the Parke Davis group³⁵ for another series of kinase inhibitors containing the 2,6-dichlorophenyl moiety, though in that series the dichlorophenyl is attached directly to the core.

The SAR involving the phenyl ring is consistent with the proposed model. The chlorines at both two and six make specific hydrophobic interactions with Val323, Leu325, Phe405, and with the hydrophobic portion of Lys295 (see Figure 5). One of the chlorines is in contact

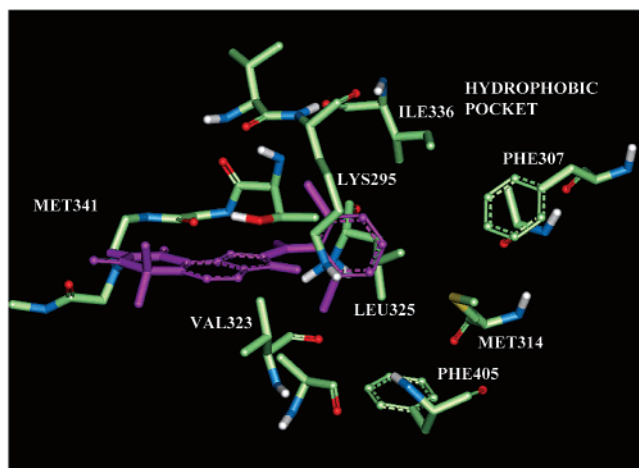


Figure 5. Details of the hydrophobic pocket of hck, with **1** bound. Only residues that contact the inhibitor are shown.

with the backbone of residues Lys295 and Ile336. These structural features explain the size limitations at the 2- and 6-position and particularly why larger groups such as ethyl (**32**) decrease potency. It is also clear from the model that substitution at C3 or C5 of the phenyl ring, as in **35**, will not be tolerated since the hydrogens at these positions in **1** are already in van der Waals contact with residues in the hydrophobic pocket. In addition, the model suggests the possibility of substitution at C4, which also correlates with the results obtained for **33** and **34**, with similar activity to **1**.

The model explains the SAR in the dichlorophenyl ring, but it also suggests that there are few possibilities for improving activity by making changes in this region. However, a more exciting opportunity was apparent in the imide ring. In the model, the geminal-methyl groups lie close to the glycine rich loop above the inhibitor and the adjacent loop of the C-terminal lobe below (Figure 6). Larger substituents cannot be accommodated, as confirmed by the weaker activity of **37** and **38**, but a substituent in the plane of the molecule would project out into the unoccupied cleft and might provide an opportunity to build in additional binding. This observation led us to design the isoquinolone **20**, which would achieve the desired planarity. We were delighted to find that **20** showed an 18-fold increase in potency in the enzyme assay, with an IC_{50} of $0.026 \mu M$, and an even greater gain in cell potency (see below). The discovery of the isoquinolone confirmed our hypothesis and provided a new class of kinase inhibitor. Analogues of **20** displayed the same improvement in potency over the corresponding imide. In this case, the monochloro analogue **39** had measurable activity but was 8-fold less potent than **20**. SAR of compounds **40–42** paralleled that of the imide series. The gain in activity of **20** seems to be due to more than simply removing the methyl groups. Although we were unable to prepare the unsubstituted analogue of **1**, we were able to make this change in the lactam **25**, which had only a modest 3-fold improvement in activity over its *gem*-dimethyl analogue **18**.

To gain a more detailed understanding of the improved activity of **20**, a model of the complex with hck was constructed. A detailed MD simulation was carried out for the complexes of both **1** and **20** with hck in water

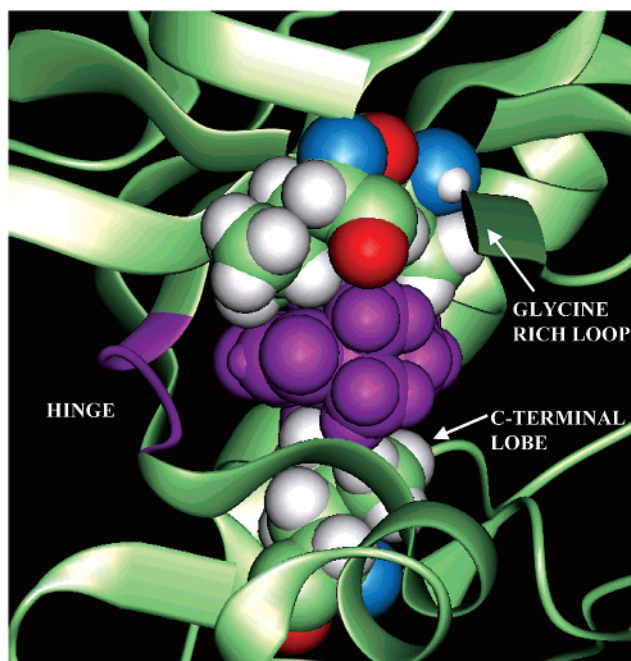


Figure 6. Interaction of the *gem*-dimethyl group of **1** with the ATP site. Compound **1** (magenta) bound into hck. The inhibitor and residues that make contact with the *gem*-dimethyl group are shown in space-filling representation.

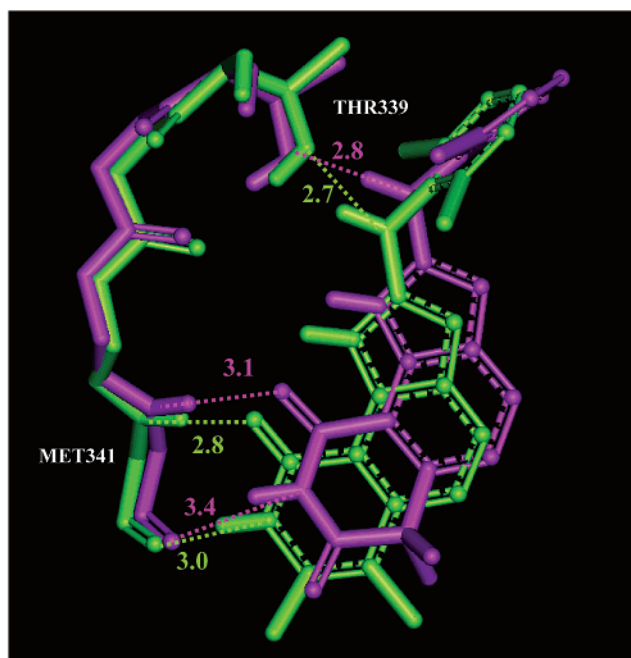
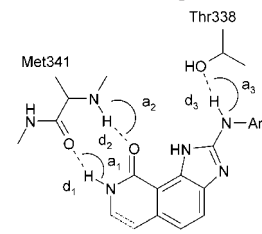


Figure 7. Overlay of the binding models of **1** and **20** from MD simulation. Mean positions of compounds **1** (magenta) and **20** (green). The backbone of the hinge region is shown in the corresponding color for each model. Dashed lines indicate H bonds for each model, with lengths in Ångstroms.

(see Experimental Section). The overlay of the average structures of the two complexes is shown in Figure 7. To understand the possible changes in intermolecular interaction that could explain the increase in activity for **20** as compared to **1**, the MD profiles for the three intermolecular hydrogen bonds were analyzed. Table 3 shows the average distances and rms deviations for these three hydrogen bonds from a 600 ps MD simulation. This reveals that **1** does not maintain three strong

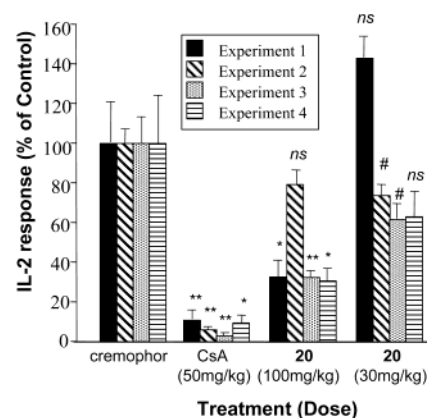
Table 3. H Bond Distances in Complexes of **1** and **20** with Hck


compd	distance (Å) (rms)			angle (deg) (rms)		
	d_1	d_2	d_3	a_1	a_2	a_3
1	3.4 (0.25)	3.1 (0.20)	2.8 (0.10)	140 (11)	156 (11)	164 (8)
20	3.0 (0.15)	2.8 (0.11)	2.7 (0.10)	147 (10)	162 (10)	131 (9)

intermolecular hydrogen bonds in a concerted manner with the two acceptors and one donor group in the protein surface. The bond from the imide NH to Met341 CO in particular was longer (d_1) and showed more variation in distance. From this analysis, it was concluded that the inhibitor could not bind deeply enough in the hydrophobic pocket to allow optimum hydrogen bond distances. In contrast, **20** maintains three consistent hydrogen bonds during the time frame of the simulation. The hydrogen bond between the exocyclic NH of the inhibitor and the oxygen of Thr338 appears to be the strongest interaction. However, the average donor-acceptor angle (131°) is smaller than that of the other two bonds, which are more nearly linear. Compound **1** also shows a strong hydrogen bond with Thr338, but the remaining hydrogen bonds are much weaker than the corresponding interactions observed for **20**. From this analysis, we conclude that the gain in activity of **20** results from the removal of the steric hindrance from the *gem*-dimethyl moiety, which in turn allows the inhibitor to bind closer to the hinge region. This is indicated by the shorter H bonds but also results in a better van der Waals interaction between the inhibitor and the protein, which contributes additional binding energy.

Cellular Assays. Cellular activity was assessed using an assay of calcium mobilization in Jurkat cells, following activation of the cells by cross-linking the TCR with anti-CD3 antibody. The results for selected compounds are shown in Table 1. Compound **1** has moderate activity in this assay, but the isoquinolone **20**, $EC_{50} = 0.19 \mu\text{M}$, is 50 times more potent, an even greater improvement than that seen in the enzyme assay. The 2-chloro-6-methyl analogue **40** is equally active, but halogens at C4 of the phenyl are less well-tolerated in the cell than in the enzyme assay. Compound **20** was further tested in an IL-2 inhibition assay, also in Jurkat cells, where it inhibited with $EC_{50} = 1 \mu\text{M}$. This assay uses anti-CD3 antibody in combination with PMA as stimulus and a buffer containing 10% serum. The calcium assay does not contain serum, and the decrease in potency in the IL-2 assay is thought to be due to protein binding of the inhibitor.

In Vivo Activity. Because **20** showed activity in an in vitro assay of IL-2 inhibition, the compound was tested for its ability to inhibit IL-2 production in a mouse assay, following stimulation of the T cells by administering anti-CD3 antibody (Figure 8). In 3 out of 4 experiments, **20** showed significant inhibition of IL-2 production at a dose of 100 mg/kg ip. The inhibition

**Figure 8.** Inhibition of IL-2 production in mice. Data from four separate experiments. CsA, cyclosporin A; **, $p < 0.001$; *, $p < 0.01$; #, $p < 0.05$; ns, not significant. Error bars indicate SEM.**Table 4.** Selectivity Profile of Compound **20**

kinase	IC_{50} (μM) ^a or highest dose tested	kinase	IC_{50} (μM) ^a or highest dose tested
Lck	0.026	Syk	> 100
c-src	0.012	EGFR	~100
ZAP70	~80	p38	no inhibition at 10 $\mu\text{g/mL}$
PKA	no inhibition at 500 μM	Erk	no inhibition at 100 $\mu\text{g/mL}$

^a In each case, the ATP was less than or equal to the apparent K_m .

was not statistically significant at 30 mg/kg. No inhibition was seen with oral dosing. This result indicates that in vivo activity can be achieved with this series of compounds and provided the impetus for further work to achieve oral activity.

Selectivity. Selectivity among the many kinases will be important for developing a therapeutic agent. With this in mind, we examined the selectivity profile of **20** against a number of other kinases (Table 4). Little, if any, inhibition was seen with a receptor tyrosine kinase, EGFR, the nonreceptor tyrosine kinases ZAP70 and syk, or with the serine/threonine kinases p38 and Erk. Inhibition of c-src was comparable to lck, which is not surprising in view of the close homology of the binding sites of the two enzymes noted above. In each case, the ATP concentration was $1 \mu\text{M}$, which is below its apparent K_m (4 and $9.8 \mu\text{M}$ for lck and c-src, respectively). Under these conditions, the relative IC_{50} values give a good indication of selectivity. Src itself has been of interest as a therapeutic target for both cancer and osteoporosis.¹⁷ From these data, **20** shows an encouraging level of selectivity for the src family over a variety of other kinases.

Conclusions

This paper highlights the utility of molecular modeling in understanding and improving the activity of a screening hit. This analysis led to a new structural class of kinase inhibitor, exemplified by **20**. Eighteen-fold increases in potency against the enzyme and 50-fold increases in cellular potency were realized. The demonstration of in vivo activity highlights the potential of this series for further optimization. This will be the subject of future papers.

Experimental Section

Melting points were determined with an Electrothermal capillary melting point apparatus or a Fisher-Johns Apparatus and are uncorrected. Proton NMR (^1H NMR) spectra were recorded on a Bruker Avance 400 or a Bruker AF270 spectrometer operating at 400 and 270 MHz, respectively. Chemical shifts are reported as δ values in parts per million, using the solvent peak as an internal reference. Electron impact mass spectra (EIMS) were run on a Finnigan SSQ7000 instrument at 70 eV. Chemical ionization mass spectra (CIMS) were run on the same machine, with NH_3 as reagent gas. Electrospray mass spectra (ESMS) were run on a MicroMass Platform LCZ instrument, at a cone voltage of 30 V. Infrared (FTIR) spectra were recorded on a Nicolet Impact 1000 machine and are of KBr disks. Flash column chromatography was carried out on silica gel (230–400 mesh). Organic solutions that had been in contact with water were dried over MgSO_4 or Na_2SO_4 , prior to concentration in a rotary evaporator. Elemental analyses were performed by QTI-Quantitative Technologies, Whitehouse, NJ.

2-(2-Cyanophenyl)-2,4-dimethylpentanonitrile (3c). To a mechanically stirred suspension of **2** (14.2 g, 0.100 mol) and benzyl tributylammonium bromide (1.07 g, 3.00 mmol) in 50% w/w sodium hydroxide solution (70 mL) was added 1-iodo-2-methyl propane (19.3 g, 0.105 mol). External cooling was used to maintain a temperature of 20–25 °C. After 2 h, NMR of a worked-up aliquot showed no **2** remaining. Methyl iodide (7.5 mL, 0.12 mol) was added, and stirring was continued for 22 h. The mixture was poured onto ice, extracted with EtOAc, and evaporated to give **3c** as a red oil. ^1H NMR (CDCl_3): δ 0.76 (3H, d, $J = 7$ Hz), 0.99 (3H, d, $J = 7$ Hz), 1.58–1.64 (1H, m), 1.96–2.02 (1H, m), 1.98 (3H, s), 2.55 (1H, dd, $J = 6$ and 14 Hz), 7.45 (1H, t, $J = 8$ Hz), 7.64 (1H, t, $J = 8$ Hz), 7.75 (1H, d, $J = 8$ Hz), 7.91 (1H, d, $J = 8$ Hz).

4-Methyl-4-(2-methylpropyl)-2H,4H-isoquinoline-1,3-dione (4c). A solution of crude **3c** (12.7 g, 60 mmol) in 90% H_2SO_4 was stirred at room temperature for 64 h and then at 60 °C for 24 h. The cooled solution was poured onto ice and extracted with EtOAc. The extracts were washed with water and brine and evaporated. NMR indicated a 5:1 mixture of **5c** and **4c**. A pure sample of **5c** was isolated by column chromatography in hexane/EtOAc, 3:1 from a separate run. CIMS: m/z 233 (MH^+). IR: 1750, 1800 cm^{-1} . A stirred solution of the crude product in THF (100 mL) and NH_4OH (50 mL) was heated to 65 °C. After 3 h, more NH_4OH (50 mL) was added, and heating was continued for 24 h. The solution was cooled, and most of the THF was evaporated. An amount of 3 M NaOH (60 mL) was added, and the resulting solution was decolorized with charcoal and filtered. The filtrate was neutralized with solid NH_4Cl , extracted with EtOAc, and evaporated to give **4c** (10.4 g, 74%).

4-Methyl-4-(2-methylpropyl)-7-nitro-2H,4H-isoquinoline-1,3-dione (6c). Solid **4c** (9.5 g, 41.1 mmol) was added portionwise to a vigorously stirred mixture of concentrated H_2SO_4 (50 mL) and concentrated HNO_3 (50 mL) at 0–5 °C. After 1 h, the mixture was poured onto ice, filtered, washed well with water, and dried to give **6c** (10.3 g, 90%).

4,4-Dimethyl-7-nitro-2H,4H-isoquinoline-1,3-dione (6a). Yield, 93%; mp 226–227 °C. ^1H NMR (acetone- d_6): δ 1.63 (6H, s), 7.98 (1H, dd $J = 5$ and 9 Hz), 8.45 (1H, dd $J = 2$ and 9 Hz), 8.75 (1H, dd $J = 2$ and 5 Hz), 11.10 (1H, s).

7-Acetamido-4,4-dimethyl-8-nitro-2H,4H-isoquinoline-1,3-dione (7a). A solution of **6a**, prepared as described for **6c**, (1.0 g, 4.5 mmol) in methanol (50 mL) was hydrogenated over 10% Pd/C (30 mg) at 50 psi for 1.5 h. The catalyst was removed by filtration, and the solvent was removed to give the amine (0.90 g, 98%). The amine (1.50 g, 7.35 mmol) was stirred in acetic anhydride (9 mL) at room temperature for 3 h and then poured on to ice. The precipitate was filtered, washed with water, and dried to give the acetamide (1.55 g, 86%). The amide was converted to **7a** as previously described;²⁰ yield, 80%; mp 267–268 °C. ^1H NMR (dimethyl sulfoxide (DMSO)- d_6): δ 1.57 (6H, s), 2.04 (3H, s), 7.92 (2H, s), 9.86 (1H, s), 11.61 (1H, s). CIMS: m/z 291 (MH^+).

7-Amino-4,4-dimethyl-8-nitro-2H,4H-isoquinoline-1,3-dione (8a). Compound **7a** (4.0 g, 13.7 mmol) was added to 90% H_2SO_4 and heated at 70 °C for 8 h. The cooled mixture was poured onto ice. The precipitate was collected, dissolved in EtOAc, washed with water, dried, and evaporated to give **8a** (3.38 g, 99%); mp 259–263 °C. ^1H NMR (CDCl_3): δ 1.28 (6H, s), 4.87 (2H, br), 6.96 (1H, d, $J = 9$ Hz), 7.06 (1H, d, $J = 9$ Hz), 10.05 (1H, s). CIMS: m/z 250 (MH^+).

7,8-Diamino-4,4-dimethyl-2H,4H-isoquinoline-1,3-dione (9a). A solution of **8a** (1.5 g, 6.0 mmol) in methanol (50 mL) was hydrogenated over platinum oxide (30 mg) at 50 psi for 1.25 h. The mixture was filtered through Celite and evaporated to provide **9a** (1.31 g, 100%). ^1H NMR (CDCl_3): δ 1.58 (6H, s), 3.34 (2H, br), 6.12 (2H, br), 6.66 (1H, d, $J = 9$ Hz), 6.91 (1H, d, $J = 9$ Hz), 8.25 (1H, s). CIMS: m/z 220 (MH^+).

1-(8-Amino-4,4-dimethyl-1,3-dioxo-1,2,3,4-tetrahydroisoquinolin-7-yl)-3-(2,6-dichlorophenyl)thiourea (10a). 2,6-Dichlorophenylisothiocyanate (1.16 g, 5.7 mmol) was added to a suspension of **9a** (1.31 g, 6.0 mmol) in EtOAc (40 mL), and the mixture was stirred overnight. The solid was filtered and dried to yield the thiourea (1.55 g, 61%); mp > 300 °C. ^1H NMR ($\text{MeOH}-d_4$): δ 1.62 (6H, s), 6.86 (1H, d, $J = 8$ Hz), 7.34 (1H, t, $J = 8$ Hz), 7.45 (1H, d, $J = 8$ Hz), 7.49 (2H, d, $J = 8$ Hz). CIMS: m/z 423, 425 (MH^+).

2-(2,6-Dichlorophenylamino)-6,6-dimethyl-1H,6H-imidazo[4,5-*h*]isoquinoline-7,9-dione (1). A solution of thiourea **10** (2.23 g, 5.28 mmol) in THF (50 mL) and dicyclohexylcarbodiimide (1.11 g, 5.4 mmol) was heated under reflux with stirring for 4 h. The cooled solution was stirred overnight and filtered, and the crystals were washed with CH_2Cl_2 to give **1** (1.20 g). The filtrate was evaporated and triturated with CH_2Cl_2 to give more product (0.7 g, 93% combined yield); mp 290–292 °C. ^1H NMR ($\text{DMSO}-d_6$): δ 1.55 (6H, s), 7.24 (1H, d, $J = 8$ Hz), 7.36 (1H, t, $J = 8$ Hz), 7.51 (1H, d, $J = 8$ Hz), 7.59 (2H, d, $J = 8$ Hz), 8.47 (1H, s), 11.34 (1H, s). EIMS: m/z 388, 390 (M^+). Anal. ($\text{C}_{18}\text{H}_{14}\text{Cl}_2\text{N}_4\text{O}_2$) C, H, N.

2-(2-Chlorophenylamino)-6,6-dimethyl-1H,6H-imidazo[4,5-*h*]isoquinoline-7,9-dione (26). Yield, 93%; mp > 300 °C. ^1H NMR ($\text{DMSO}-d_6$): δ 1.57 (6H, s), 7.01 (1H, ddd, $J = 1, 8$ and 8 Hz), 7.34 (1H, d, $J = 8$ Hz), 7.40 (1H, ddd, $J = 1, 8$ and 8 Hz), 7.49 (1H, dd, $J = 1$ and 8 Hz), 7.75 (1H, d, $J = 8$ Hz), 8.93 (1H, dd, $J = 1$ and 8 Hz), 9.12 (1H, s), 11.37 (1H, s), 12.02 (1H, s). CIMS: m/z 355, 357 (M^+). Anal. ($\text{C}_{18}\text{H}_{15}\text{ClN}_4\text{O}_2$) C, H, N.

2-(4-Chlorophenylamino)-6,6-dimethyl-1H,6H-imidazo[4,5-*h*]isoquinoline-7,9-dione (28). Yield, 86%; mp > 300 °C. ^1H NMR ($\text{DMSO}-d_6$): δ 1.57 (6H, s), 7.32 (1H, d, $J = 8$ Hz), 7.40 (2H, dd, $J = 2$ and 7 Hz), 7.71 (1H, d, $J = 8$ Hz), 7.81 (2H, dd, $J = 2$ and 7 Hz), 9.39 (1H, s), 11.21 (1H, s), 11.37 (1H, s). CIMS: m/z 355, 357 (M^+). Anal. ($\text{C}_{18}\text{H}_{15}\text{ClN}_4\text{O}_2$) C, H, N.

2-(2-Chloro-6-methylphenylamino)-6,6-dimethyl-1H,6H-imidazo[4,5-*h*]isoquinoline-7,9-dione (29). mp > 300 °C. ^1H NMR ($\text{DMSO}-d_6$): δ 1.54 (6H, s), 2.28 (3H, s), 7.22 (1H, d, $J = 8$ Hz), 7.23 (1H, t, $J = 7$ Hz), 7.29 (1H, d, $J = 7$ Hz), 7.40 (1H, d, $J = 7$ Hz), 7.48 (1H, d, $J = 8$ Hz), 8.28 (1H, s), 11.31 (1H, s), 11.33 (1H, s). CIMS: m/z 369 (MH^+). Anal. ($\text{C}_{19}\text{H}_{17}\text{ClN}_4\text{O}_2 \cdot 1.1\text{H}_2\text{O}$) C, H, N.

2-(2,6-Dimethylphenylamino)-6,6-dimethyl-1H,6H-imidazo[4,5-*h*]isoquinoline-7,9-dione (30). Yield, 81%; mp > 300 °C. ^1H NMR ($\text{DMSO}-d_6$): δ 1.54 (6H, s), 2.22 (6H, s), 7.11–7.12 (3H, m), 7.19 (1H, d, $J = 8$ Hz), 7.43 (1H, d, $J = 8$ Hz), 8.04 (1H, s), 11.16 (1H, s), 11.31 (1H, s). CIMS: m/z 349 (M^+). Anal. ($\text{C}_{20}\text{H}_{20}\text{ClN}_4\text{O}_2 \cdot 0.3\text{H}_2\text{O}$) C, H, N.

2-(2,4,6-Trichlorophenylamino)-6,6-dimethyl-1H,6H-imidazo[4,5-*h*]isoquinoline-7,9-dione (33). mp > 275 °C. ^1H NMR ($\text{DMSO}-d_6$, 115 °C): δ 1.58 (6H, s), 7.21 (1H, d, $J = 8$ Hz), 7.45 (1H, d, $J = 8$ Hz), 8.5–9 (1H, v. br), 10.5–11 (2H, v. br). CIMS: m/z 423, 425, 427 (MH^+). Anal. ($\text{C}_{18}\text{H}_{13}\text{Cl}_3\text{N}_4\text{O}_2$) C, H, N.

2-(2,6-Dichlorophenylamino)-6,6,8-trimethyl-1H,6H-imidazo[4,5-*h*]isoquinoline-7,9-dione (11). To a stirred solution of **1** (100 mg, 0.257 mmol) in DMSO (1 mL) was added a 1 M solution of sodium hexamethyldisilazide in THF (0.28

mL, 0.28 mmol). After it was stirred at room temperature for 20 min, methyl iodide (20 μ L, 0.30 mmol) was added, and stirring was continued for 1 h. The solution was diluted with water and extracted with CH_2Cl_2 . Flash chromatography in $\text{CH}_2\text{Cl}_2/\text{MeOH}$ (99:1) gave **11** (31 mg) as the second eluted component. Crystallization from CH_2Cl_2 containing a little MeOH, by slow evaporation, yielded pure **11** (20 mg, 19%); mp 287–290 °C. $^1\text{H NMR}$ (DMSO- d_6): δ 1.58 (6H, s), 3.28 (3H, s), 7.24 (1H, d, $J = 8$ Hz), 7.36 (1H, t, $J = 8$ Hz), 7.51 (1H, d, $J = 8$ Hz), 7.58 (2H, d, $J = 8$ Hz), 8.46 (1H, s), 11.44 (1H, s). CIMS: m/z 403 (MH^+). Anal. ($\text{C}_{19}\text{H}_{16}\text{Cl}_2\text{N}_4\text{O}_2$) C, H, N.

2-(2,6-Dichlorophenylamino)-3,6,6,8-tetramethyl-3H,6H-imidazo[4,5-*h*]isoquinoline-7,9-dione (12) and 2-(N,2,6-Dichlorophenyl-*N*-methylamino)-6,6,8-trimethyl-1H,6H-imidazo[4,5-*h*]isoquinoline-7,9-dione (13). Compounds **12** and **13** were acquired following the procedure described for **11** but using sodium hydride (17 mg, 0.39 mmol) and methyl iodide (32 μ L, 0.51 mmol). Flash chromatography in $\text{CH}_2\text{Cl}_2/\text{MeOH}$ (99:1) gave **12** (52 mg) as the first eluted component and **13** (23 mg) as the second eluted component. Compound **12** was further purified by chromatography in $\text{CH}_2\text{Cl}_2/\text{EtOAc}$ (95:5) and crystallization from EtOAc/hexane; yield, 24 mg; mp 235–237 °C. $^1\text{H NMR}$ (CDCl_3): δ 1.63 (6H, s), 3.31 (3H, s), 3.61 (3H, s), 6.98 (1H, t, $J = 8$ Hz), 7.13 (1H, d, $J = 8$ Hz), 7.17 (1H, d, $J = 8$ Hz), 7.37 (2H, d, $J = 8$ Hz), 8.8–9.1 (1H, v. br). CIMS: m/z 417 (MH^+). Anal. ($\text{C}_{20}\text{H}_{18}\text{Cl}_2\text{N}_4\text{O}_2$) C, H, N.

Compound **13** had mp 228–233 °C. $^1\text{H NMR}$ (CDCl_3): δ 1.67 (6H, s), 3.34 (3H, s), 3.61 (3H, s), 7.25 (1H, d, $J = 8$ Hz), 7.41 (1H, t, $J = 8$ Hz), 7.55 (2H, d, $J = 8$ Hz), 7.81 (1H, d, $J = 8$ Hz), 9.40 (1H, br). EIMS: m/z 416 (M^+).

2-(2,6-Dichlorophenylamino)-3,6,6-trimethyl-1H,6H-imidazo[4,5-*h*]isoquinoline-7,9-dione (14), 2-(2,6-Dichlorophenylmethylamino)-6,6-dimethyl-1H,6H-imidazo[4,5-*h*]isoquinoline-7,9-dione (15), and 2-(2,6-Dichlorophenylmethylamino)-3,6,6-trimethyl-1H,6H-imidazo[4,5-*h*]isoquinoline-7,9-dione (16). To a stirred solution of **1** (550 mg, 1.41 mmol) in dry dimethyl formamide (DMF, 2.5 mL) was added CH_3I (2.5 mL, 40 mmol). The reaction vessel was sealed, and the contents were stirred at room temperature for 16 h. The CH_3I was evaporated, and the resulting solution was diluted with 25 mL of saturated NaHCO_3 and allowed to stir for 3 h. The product was filtered, washed with H_2O , and then slurried in CHCl_3 . The insolubles were filtered, and the mother liquors were evaporated to leave 480 mg of a mixture of **14**–**16**. Flash chromatography using a gradient (25% EtOAc in hexane–100% EtOAc) gave **14** (130 mg, 23%), **15** (100 mg, 18%), and **16** (73 mg, 13%). Compound **14**: mp 128–132 °C. $^1\text{H NMR}$ (CDCl_3): δ 1.69 (6H, s), 3.63 (3H, s), 6.99 (1H, t, $J = 8$ Hz), 7.15–7.22 (2H, m), 7.40 (2H, d, $J = 8$ Hz), 8.08 (1H, s), 8.85 (1H, s). CIMS: m/z 403, 405 (MH^+). Anal. ($\text{C}_{19}\text{H}_{16}\text{Cl}_2\text{N}_4\text{O}_2$) C, H, N.

Further purification by flash chromatography (2% CH_3OH in CH_2Cl_2) yielded **15**; mp 284–286 °C. $^1\text{H NMR}$ (CDCl_3): δ 1.70 (6H, s), 3.58 (3H, s), 7.24 (1H, d, $J = 8$ Hz), 7.39 (1H, t, $J = 8$ Hz), 7.55 (2H, d, $J = 8$ Hz), 7.83 (1H, d, $J = 8$ Hz), 8.43 (1H, s), 9.30 (1H, br). CIMS: m/z 403, 405 (MH^+). Anal. ($\text{C}_{19}\text{H}_{16}\text{Cl}_2\text{N}_4\text{O}_2 \cdot 0.3\text{H}_2\text{O}$) C, H, N.

Crystallization from EtOAc containing a little MeOH, by slow evaporation, yielded pure **16**; mp 261–263 °C. $^1\text{H NMR}$ (CD_3OD + few drops of CDCl_3): δ 1.63 (6H, s), 3.01 (3H, s), 3.57 (3H, s), 7.27 (1H, d, $J = 7$ Hz), 7.38 (1H, t, $J = 7$ Hz), 7.46 (1H, d, $J = 7$ Hz), 7.54 (2H, d, $J = 7$ Hz). CIMS: m/z 417, 419 (MH^+). Anal. ($\text{C}_{20}\text{H}_{18}\text{Cl}_2\text{N}_4\text{O}_2 \cdot 0.4\text{H}_2\text{O}$) C, H, N.

2-(2,6-Dichlorophenylamino)-6,6-dimethyl-7,8-dihydro-1H,6H-imidazo[4,5-*h*]isoquinoline-9-one (18). To a solution of **1** (90 mg, 0.23 mmol) in THF (5 mL) was added NaBH_4 (90 mg, 2.3 mmol) followed by water (4 drops). The reaction mixture was stirred at ambient temperature for 1 h. Subsequently, 1 N HCl (5 mL) was added dropwise and the reaction mixture was stirred an additional 15 min, neutralized with NaHCO_3 , and extracted with EtOAc. The extract was washed with brine and evaporated yielding alcohol **17** (90 mg, 99%). $^1\text{H NMR}$ (CD_3OD): δ 1.31 (3H, s), 1.50 (3H, s), 4.72 (1H, s), 7.13 (1H, d, $J = 8$ Hz), 7.28 (1H, t, $J = 8$ Hz), 7.40 (1H, d, $J =$

8 Hz), 7.51 (2H, d, $J = 8$ Hz). This unstable intermediate was used immediately. It was further characterized as the methyl ether, which was prepared by dissolving **17** (20 mg, 0.05 mmol) in MeOH/HCl and stirring for several hours. After it was evaporated, the residue was partitioned between EtOAc/aqueous NaHCO_3 . The organic phase was washed with brine, dried, and evaporated to the methyl ether derivative (15.6 mg, 75%); mp 278–280 °C (dec). $^1\text{H NMR}$ (CD_3OD): δ 1.30 (3H, s), 1.50 (3H, s), 3.37 (3H, s), 4.29 (1H, s), 7.08 (1H, d, $J = 8$ Hz), 7.28 (1H, t, $J = 8$ Hz), 7.37 (1H, d, $J = 8$ Hz), 7.51 (2H, d, $J = 8$ Hz). ESMS: m/z 405, 407 (MH^+). Compound **17** (100 mg, 0.26 mmol) was dissolved in TFA (2 mL), and this solution was added to a solution of sodium trifluoroacetoxymethylborohydride (generated in-situ from 160 mg, 4.2 mmol of NaBH_4 , and 3 mL of TFA) at 0 °C. The reaction mixture was stirred at ambient temperature for 4 h, the solvent was evaporated, the residue was triturated with water, and the resultant mixture was neutralized with NaHCO_3 and filtered yielding **18** (85 mg, 92%). This product was further purified by flash chromatography using 4% MeOH/ CH_2Cl_2 as eluant and recrystallized from EtOAc; mp 287–290 °C. $^1\text{H NMR}$ (CDCl_3): δ 1.41 (6H, s), 3.38 (2H, d, $J = 3$ Hz), 6.22 (1H, s), 7.09 (1H, d, $J = 8$ Hz), 7.17 (1H, t, $J = 8$ Hz), 7.44 (2H, d, $J = 8$ Hz), 7.56 (1H, d, $J = 8$ Hz), 10.12 (1H, br). CIMS: 375, 377 (MH^+). Anal. ($\text{C}_{18}\text{H}_{16}\text{Cl}_2\text{N}_4\text{O} \cdot 0.2\text{H}_2\text{O}$) C, H, N.

(2,6-Dichlorophenyl)-(6,6-dimethyl-6,7,8,9-tetrahydro-3H-imidazo[4,5-*h*]isoquinolin-2-yl)amine (19). To a solution of **17** (180 mg, 0.46 mmol) in THF (15 mL) was added NaBH_4 (180 mg, 4.6 mmol) followed by a solution of TFA (1 mL) in THF (5 mL). This was repeated 5 \times over a 48 h period until the absence of **17** was indicated by thin-layer chromatography (TLC). Subsequently, 1 N HCl (5 mL) was added dropwise and the reaction mixture was stirred an additional 15 min, the organic solvents were evaporated, and the aqueous residue was neutralized with NaHCO_3 and extracted with EtOAc. The extract was washed with brine and evaporated yielding a mixture of **18** and **19**. This mixture was purified by flash chromatography using 4% MeOH/ CH_2Cl_2 as eluant. Compound **19** was further purified by high-performance liquid chromatography (HPLC) using 70% CH_3CN – H_2O with 1% TFA as eluant. Compound **19** was isolated as a TFA salt (25 mg, 10%); mp > 300 °C (dec). $^1\text{H NMR}$ (CD_3OD): δ 1.39 (3H, s), 1.41 (3H, s), 2.77 (1H, d, $J = 12$ Hz), 3.15 (1H, d, $J = 12$ Hz), 3.84 (1H, d, $J = 16$ Hz), 4.38 (1H, d, $J = 16$ Hz), 7.35 (1H, d, $J = 8$ Hz), 7.47 (1H, d, $J = 8$ Hz), 7.56 (1H, t, $J = 8$ Hz), 7.69 (2H, d, $J = 8$ Hz). CIMS: m/z 361, 363 (M^+). Anal. ($\text{C}_{18}\text{H}_{18}\text{Cl}_2\text{N}_4 \cdot 1.7\text{TFA}$) C, H, N.

2-(2,6-Dichlorophenylamino)-6,7-dimethyl-1,8-dihydro-imidazo[4,5-*h*]isoquinoline-9-one (20). Alcohol **17** (45 mg, 0.11 mmol) was suspended in concentrated H_2SO_4 (1 mL), and the resultant mixture was stirred at ambient temperature for 15 min. The solution was poured over ice, neutralized with NaHCO_3 , and filtered. The filtrate was triturated with water (10 mL) and centrifuged. The liquid was decanted, and the residual solid was triturated with methanol and centrifuged. The supernatant was decanted, and the residue was dried to give **20** (35 mg, 84%); mp > 300 °C. $^1\text{H NMR}$ (DMSO- d_6): δ 2.20 (3H, s), 2.28 (3H, s), 7.29–7.36 (2H, m), 7.57–7.61 (3H, m), 8.46 (1H, s), 11.23 (1H, s), 11.43 (1H, s). ESMS: m/z 373, 375 (M^+). Anal. ($\text{C}_{18}\text{H}_{14}\text{Cl}_2\text{N}_4\text{O} \cdot 0.3\text{H}_2\text{O}$) C, H, N.

2-(2-Chlorophenylamino)-6,7-dimethyl-1,8-dihydro-imidazo[4,5-*h*]isoquinoline-9-one (39). Yield, 84%; mp > 300 °C. $^1\text{H NMR}$ (DMSO- d_6): δ 2.23 (3H, s), 2.29 (3H, s), 6.99 (1H, dd, both $J = 8$ Hz), 7.40 (2H, m), 7.48 (1H, d, $J = 8$ Hz), 7.83 (1H, d, $J = 8$ Hz), 8.98 (1H, d, $J = 8$ Hz), 9.13 (1H, s), 11.26 (1H, s), 12.18 (1H, br). CIMS: m/z 339, 341 (M^+). Anal. ($\text{C}_{18}\text{H}_{15}\text{ClN}_4\text{O} \cdot 0.4\text{H}_2\text{O}$) C, H, N.

7-Acetamido-8-nitro-3,4-dihydro-2H-isoquinoline-1-one (22). Compound **22** was prepared from **21**²³ by the sequence described for **7a**. $^1\text{H NMR}$ (DMSO- d_6 , 400 MHz): δ 2.04 (3H, s), 3.32 (2H, t, $J = 6$ Hz), 4.39 (2H, t, $J = 6$ Hz), 7.61 (1H, d, $J = 9$ Hz), 7.84 (1H, d, $J = 9$ Hz), 8.03 (1H, s), 9.88 (1H, s).

7-Acetamido-8-amino-3,4-dihydro-2H-isoquinoline-1-one (23). A 1 L round bottom flask with mechanical stirrer was charged with **22** (14.2 g, 57.0 mmol), iron powder (19.1 g, 342 mmol), 95% EtOH (250 mL), and concentrated HCl (1.0 mL). The mixture was stirred and heated to reflux under N₂ for 3 h. The mixture was cooled to room temperature and was passed through a pad of silica gel with MeOH wash (4×). The filtrate was concentrated in vacuo. The residue was dissolved in MeOH and passed through a pad of silica gel again, with MeOH wash (4×). The filtrate was concentrated in vacuo to obtain **23** as a yellow solid (11.0 g 88%). ¹H NMR (DMSO-*d*₆): δ 2.05 (3H, s), 2.84 (2H, t, *J* = 3 Hz), 3.35 (2H, t, *J* = 3 Hz), 7.22 (1H, d, *J* = 9 Hz), 7.69 (1H, d, *J* = 9 Hz), 7.87 (1H, s), 8.03 (1H, s), 10.02 (1H, s).

2-(2,6-Dichlorophenylamino)-6,7-dihydro-1H,8H-imidazo[4,5-*h*]isoquinoline-9-one (25). A mixture of **23** (219 mg, 1.0 mmol) and hydrazine hydrate (55%, 6 mL) was heated at 90 °C with stirring overnight. The solvent was evaporated to complete dryness under high vacuum. The resulting yellow solid was used directly for the next step without purification. To the residue was added DMF (7 mL) and 2,6-dichlorophenyl isothiocyanate (204 mg, 1.0 mmol), and the mixture was stirred for 60 h at room temperature. The mixture was diluted with water (15 mL) and extracted with EtOAc (4×). The EtOAc layers were combined, dried over Na₂SO₄, and concentrated in vacuo. The residue was purified by flash chromatography (silica gel, 0–15% MeOH/EtOAc) to afford the thiourea as a white solid (61 mg, 16%). ¹H NMR (DMSO-*d*₆): δ 2.79 (2H, t, *J* = 7.0 Hz), 3.29 (2H, t, *J* = 7.0 Hz), 6.46 (1H, d, *J* = 7.8 Hz), 6.55 (2H, br s), 7.12 (2H, d, *J* = 7.2 Hz), 7.32 (2H, t, *J* = 8.1 Hz), 7.50 (2H, d, *J* = 8.1 Hz), 7.81 (1H, s), 9.30 (2H, br s). A suspension of the thiourea (20 mg, 0.0525 mmol) and dicyclohexylcarbodiimide (12 mg, 0.0577 mmol) in THF (0.8 mL) was heated at 64 °C for 20 h. The cooled mixture was purified by flash chromatography (silica gel, 0–5% MeOH/EtOAc) to give **25** (12 mg, 67%) as a white solid. ¹H NMR (DMSO-*d*₆, *T* = 116 °C): δ 2.91 (2H, m), 3.40 (2H, m), 6.87 (1H, d, *J* = 7.7 Hz), 7.23 (1H, d, *J* = 7.7 Hz), 7.29 (1H, t, *J* = 7.9 Hz), 7.55 (2H, d, *J* = 8.0 Hz), 7.90 (1H, s), 8.55 (1H, brs), 10.95 (1H, brs). ¹³C NMR (DMSO-*d*₆, 100 MHz, *T* = 116 °C): δ 182.1, 165.6, 151.8, 132.7, 132.2, 130.6, 128.7, 127.5, 119.1, 118.1, 111.0, 40.0, 27.3. ESMS: *m/z* 347, 349 (MH⁺). Anal. (C₁₆H₁₂Cl₂N₄O·0.2H₂O) C, H, N.

Molecular Modeling. The docking experiments were performed using the Autodock package version 2.0,^{28,29} using coordinates from the published X-ray crystal structure of hck.²⁵ The steric grid representing the protein was computed using the default Autodock force field; 6–12 Lennard–Jones parameters for chlorine were added using the standard Amber force field.³⁰ The electrostatic Autodock grid was computed using charMM extended atom force field charges.³⁶ The grid was defined as a 30 Å × 30 Å × 30 Å box centered in the center of mass of the ligand molecule from the quercetin/hck or ADPNP/hck X-ray crystal structure. The geometry of the inhibitors were optimized with an ab initio method using a 6-31G* basis set.³⁷ The electrostatic ESP charges were then computed using the CHELPG option in Gaussian94³¹ using a 6-31G** basis set. Fifty Autodock runs of 100 000 Monte Carlo steps were performed, and the top 50 orientations were selected for further analysis. Molecular dynamics simulations of the protein/inhibitor complex were performed using the charMM program from Acclerys Inc.³⁸ The all-atoms force field was used in the simulations with the explicit TIP3P water molecule model.³⁹ Solvent effect was represented using a 25 Å water sphere (cup model). The center of the sphere was located at the center of mass of the inhibitor. All of the atoms within 13 Å of the inhibitor were free to move during the simulation. The rest of the atoms in the protein were tethered using a force constant of 1 kcal mol⁻¹ Å⁻³. The water molecules located further than 13 Å were maintained within the water sphere using the DROP charMM command with default values. The nonbonding van der Waals interactions were computed using a switch cutoff function from 9 to 11 Å and a complete cutoff from 11 Å. The nonbonding electrostatic energy was computed

using a dielectric constant of 1. A shift cutoff function from 9 to 11 Å and a complete cutoff from 11 Å were used. All MD simulations were carried out with charMM at 298 K using a time step of 0.001 ps. Heating of the system was done at a rate of 1 K every 10 MD steps. Equilibration was performed over 30 000 MD steps (30 ps). MD production was carried out for 600 ps. Energy minimization was performed using charMM with the ABNR minimizer and convergence criterion of 0.001.

Tyrosine Kinase Inhibition Assay. Inhibition of lck activity was measured using recombinant human lck kinase domain, expressed as a GST fusion in insect cells. The enzyme dose employed for lck (1–2 ng/well) as well as for all kinases tested was selected based on the ability to achieve a linear response for the entire reaction period. Buffer: 50 mM HEPES, pH 7.5, 50 mM KCl, 25 mM MgCl₂, 5 mM MnCl₂, 100 μM Na₃VO₄, 0.01% CHAPS, 1 mM DTT, and 50 μg/mL BSA, ATP stock at 100 mM (Pharmacia), γ³³P-ATP 2000 Ci/mmol stock (Perkin-Elmer), diluted to a final concentration of 1 μM and 20 Ci/mmol. The apparent *K*_m for ATP was 4 μM. Poly (L-glutamic acid-L-tyrosine, 4:1) (Fluka) utilized at 4.6 μM final concentration, equal to its apparent *K*_m. Test compound stock solutions were dissolved at 5 mg/mL in 100% DMSO. The final compound concentration for IC₅₀ determinations ranged from 200 to 1 μg/mL. The reaction was carried out in 96 well polypropylene U-bottom plates (Costar Cat no. 3794). Reactions were initiated by adding enzyme, incubated at 30 °C for 60 min, and stopped with 150 μL of 10% TCA/5% sodium pyrophosphate. The mixture was transferred to a MultiScreen-HA mixed cellulose ester membrane plate (Millipore Cat no. MHABN45), harvested by filtration, scintillation cocktail added, and radioactivity measured on a Packard Topcount instrument.

Calcium Release in Jurkat Cells. Jurkat cells were pelleted, washed 2 times with RPMI1640, 10 mM HEPES, 10% fetal bovine serum (FBS), and then resuspended at 2 × 10⁷ cells/mL. The cells were loaded with Fluo-3 solution at a final concentration of 2 μM and then washed with Hanks' Balanced Salt Solution (HBSS), containing 1 mM CaCl₂, 1 mM MgCl₂, 10 mM HEPES, 2 mM probenecid, 1% FBS, pH 7.4 (diluent). Finally, cells were suspended at 2 × 10⁷ cells/mL and 2 mL of loaded cell suspension were mixed with 18 mL of diluent. A 150 μL amount of this mixture was then added to each well of a 96 well Black Packard viewplate for a final cell number of 3 × 10⁵/mL. A 50 μL amount of diluted compound was added to the cells and incubated at room temperature for 15 min. Subsequently, 50 μL of anti-CD3, clone X35 (Immunotech), was added to the cell plate for a final concentration of 0.25 μg/mL and fluorescence intensity was monitored for an additional 13 min.

Inhibition of IL-2 Production. Ninety-six well flat bottom plates were coated with anti-CD3, clone UCHT1 (Immunotech), at 4 μg/mL in phosphate-buffered saline (PBS), 100 μL/well. The plate was then incubated at 37 °C for 2 h or overnight at 4 °C. Jurkat cells were pelleted and counted. The cells were resuspended at 2.5 × 10⁶ cells/mL in RPMI1640, 10% FBS (complete media). Test compounds were diluted from a 5 mg/mL DMSO stock directly into complete media and then added to 100 μL of cell suspension in triplicate, and this plate was preincubated at 37 °C for 30 min. The 96 well plate containing anti-CD3 was aspirated, and the cells and compound were transferred to this plate. A 100 μL amount of PMA (phorbol 12-myristate 13-acetate) at 20 ng/mL was added for a final concentration of 10 ng/mL, and the plate was incubated overnight at 37 °C. The plate was then centrifuged at 1500 rpm for 5 min at room temperature, and the supernatants were removed and tested for IL-2 production using an enzyme-linked immunosorbent assay (ELISA) (R&D Systems, Minneapolis, MN).

In Vivo Anti-CD3 Assay. Female BALB/c mice (Charles River, The Jackson Laboratories) were used for anti-CD3 studies. Animals were numbered by tail tattoo and were 6–8 weeks old at the initiation of experiments.

Induction of IL-2 in vivo by anti-CD3: 1 μg of anti-CD3 (monoclonal hamster antimouse 145-2C11, lot M03283) in 200

μL of PBS was injected intraperitoneally (ip) into experimental mice to stimulate the polyclonal activation of T cells. Upon activation, these T cells produce IL-2, which was detected in the plasma.

Measurement of plasma cytokine levels: 3 h after anti-CD3 injection, each mouse was anesthetized with isoflurane, and approximately 0.5 mL of whole blood was collected in heparinized tubes following cardiac puncture. Plasma IL-2 levels were determined by ELISA (R&D Systems) of 1:10 dilutions of samples. Levels were quantitated by linear regression analysis of samples in comparison to a recombinant cytokine IL-2 curve, and plasma levels in vehicle-treated groups were 1900–2800 pg/mL in each experiment.

Treatment groups: All doses of compounds and controls are represented as milligrams of compound per kilogram of body mass and were administered ip in 100 μL vehicle. Compound was administered to mice ($n = 8$ per group) 1 h prior to anti-CD3 injection. Control mice received either 100 μL vehicle alone (negative control) or 30 mg/kg cyclosporin A (positive control). Data are presented as mean \pm SEM.

Acknowledgment. We are grateful to Dr. Liang Tong for solving the crystal structure of compound **12**. We thank Dr. Daniel Goldberg for helpful discussions.

Supporting Information Available: Table of crystal data, intensity collection, and refinement details and tables of atomic coordinates, bond lengths and angles, anisotropic displacement coefficients, and hydrogen atom coordinates. This material is available free of charge via the Internet at <http://pubs.acs.org>.

References

- Weiss, A.; Littman, D. R. Signal transduction by lymphocyte antigen receptors. *Cell* **1994**, *76*, 263–274.
- Karnitz, L.; Sutor, S. L.; Torigoe, T.; Reed, J. C.; Bell, M. P.; McKean, D. J.; Leibson, P. J.; Abraham, R. T. Effects of p56lck deficiency on the growth and cytolytic effector function of an interleukin-2-dependent cytotoxic T cell line. *Mol. Cell. Biol.* **1992**, *12*, 4521–4530.
- Straus, D. B.; Weiss, A. Genetic evidence for the involvement of the lck tyrosine kinase in signal transduction through the T cell antigen receptor. *Cell* **1992**, *70*, 585–593.
- Levin, S. D.; Anderson, S. J.; Forbush, K. A.; Perlmutter, R. M. A dominant-negative transgene defines a role for p56lck in thymopoiesis. *EMBO J.* **1993**, *12*, 1671–1680.
- Molina, T. J.; Kishihara, K.; Siderovski, D. P.; van Ewijk, W.; Narendran, A.; Timms, E.; Wakeham, A.; Paige, C. J.; Hartmann, K. U.; Veillette, A. Profound block in thymocyte development in mice lacking p56lck. *Nature* **1992**, *357*, 161–164.
- Hanke, J. H.; Pollok, B. A.; Changelian, P. S. Role of tyrosine kinases in lymphocyte activation: targets for drug intervention. *Inflammation Res.* **1995**, *44*, 357–371.
- Smyth, M. S.; Stefanova, I.; Hartmann, F.; Horak, I. D.; Oshero, N.; Levitzki, A.; Burke, T. R. J. Non-amine based analogues of lavendustin A as protein-tyrosine kinase inhibitors. *J. Med. Chem.* **1993**, *36*, 3010–3014.
- Thakkar, K.; Geahlen, R. L.; Cushman, M. Synthesis and protein-tyrosine kinase inhibitory activity of polyhydroxylated stilbene analogues of piceatannol. *J. Med. Chem.* **1993**, *36*, 2950–2955.
- Faltynek, C. R.; Schroeder, J.; Mauvais, P.; Miller, D.; Wang, S.; Murphy, D.; Lehr, R.; Kelley, M.; Maycock, A.; Michne, W. Damnacanthol is a highly potent, selective inhibitor of p56lck tyrosine kinase activity. *Biochemistry* **1995**, *34*, 12404–12410.
- Cushman, M.; Zhu, H.; Geahlen, R. L.; Kraker, A. J. Synthesis and biochemical evaluation of a series of aminoflavones as potential inhibitors of protein-tyrosine kinases p56lck, EGFR, and p60v-src. *J. Med. Chem.* **1994**, *37*, 3353–3362.
- Burke, T. R. J.; Lim, B.; Marquez, V. E.; Li, Z. H.; Bolen, J. B.; Stefanova, I.; Horak, I. D. Bicyclic compounds as ring-constrained inhibitors of protein-tyrosine kinase p56lck. *J. Med. Chem.* **1993**, *36*, 425–432.
- Myers, M. R.; Setzer, N. N.; Spada, A. P.; Zulli, A. L.; Hsu, C.-Y.; Zilberstein, A.; Johnson, S. E.; Hook, L. E.; Jacoski, M. V. The preparation and SR of 4-(anilino), 4-(phenoxy), and 4-(thiophenoxy)-quinazolines: Inhibitors of p56(lck) and EGF-R tyrosine kinase activity. *Bioorg. Med. Chem. Lett.* **1997**, *7*, 417–420.
- Hanke, J. H.; Gardner, J. P.; Dow, R. L.; Changelian, P. S.; Brissette, W. H.; Weringer, E. J.; Pollok, B. A.; Connelly, P. A. Discovery of a novel, potent, and Src family selective tyrosine kinase inhibitor. Study of Lck- and FynT-dependent T cell activation. *J. Biol. Chem.* **1996**, *271*, 695–701.
- Arnold, L. D.; Calderwood, D. J.; Dixon, R. W.; Johnston, D. N.; Kamens, J. S.; Munschauer, R.; Rafferty, P.; Ratnofsky, S. E. Pyrrolo[2,3-d]pyrimidines containing an extended 5-substituent as potent and selective inhibitors of lck I. *Bioorg. Med. Chem. Lett.* **2000**, *10*, 2167–2170.
- Burchat, A. F.; Calderwood, D. J.; Hirst, G. C.; Holman, N. J.; Johnston, D. N.; Munschauer, R.; Rafferty, P.; Tometzki, G. B. Pyrrolo[2,3-d]pyrimidines containing an extended 5-substituent as potent and selective inhibitors of lck II. *Bioorg. Med. Chem. Lett.* **2000**, *10*, 2171–2174.
- Kraker, A. J.; Hartl, B. G.; Amar, A. M.; Barvian, M. R.; Showalter, H. D. H.; Moore, C. W. Biochemical and cellular effects of c-Src kinase-selective pyrido[2,3-d]pyrimidine tyrosine kinase inhibitors. *Biochem. Pharmacol.* **2000**, *60*, 885–898.
- Showalter, H. D.; Kraker, A. J. Small molecule inhibitors of the platelet-derived growth factor receptor, the fibroblast growth factor receptor, and Src family tyrosine kinases. *Pharmacol. Ther.* **1997**, *76*, 55–71.
- Bridges, A. J. Chemical inhibitors of protein kinases. *Chem. Rev.* **2001**, *101*, 2541–2571.
- Holck, J.-P.; Kampe, W.; Mertens, A.; Muller-Beckmann, B.; Strein, K. Neue Isochinolin-dione, Verfahren zu ihrer Herstellung und dieser Verbindungen enthaltende Arzneimittel sowie Zwischenprodukte. Boehringer Mannheim, German patent, DE 3410168, 1985.
- Austel, V.; Kutter, E.; Heider, J.; Eberlein, W.; Kobinger, W.; Lillie, C.; Diederer, W.; Haarmann, W. Imidazoisoquinolinediones and Salts Thereof. Boehringer Ingelheim. U.S. Patent 4,176,184, 1979.
- Wijnberg, J. B. P. A.; Schoemaker, H. E.; Speckamp, W. N. A regioselective reduction of gem-disubstituted succinimides. *Tetrahedron* **1978**, *34*, 179–187.
- Ben-Ishai, D.; Inbal, Z.; Warshawsky, A. Cyclic acylimines and cyclic carbinolamides II. Isoquinolones. *J. Heterocycl. Chem.* **1970**, *7*, 615–622.
- Moriarty, R. M.; Vaid, R. K.; Duncan, M. P.; Ochiai, M.; Inenaga, M.; Nagao, Y. Hypervalent Iodine Oxidation of Amines Using Iodosobenzene: Synthesis of Nitriles, Ketones and Lactams. *Tetrahedron Lett.* **1988**, *29*, 6913–6916.
- Xu, W.; Harrison, S. C.; Eck, M. J. Three-dimensional structure of the tyrosine kinase c-Src. *Nature* **1997**, *385*, 595–602.
- Sicheri, F.; Moarefi, I.; Kuriyan, J. Crystal structure of the Src family tyrosine kinase Hck. *Nature* **1997**, *385*, 602–609.
- Miertus, S.; Scrocco, E.; Tomasi, J. Electrostatic interaction of a solute with a continuum. A direct utilization of ab initio molecular potentials for the prevision of solvent effects. *Chem. Phys.* **1981**, *55*, 117–129.
- Luque, F. J.; Negre, M. J.; Orozco, M. An AM1-SCRF approach to the study of changes in molecular properties induced by solvent. *J. Phys. Chem.* **1993**, *97*, 4386–4391.
- Morris, G. M.; Goodsell, D. S.; Huey, R.; Olson, A. J. Distributed automated docking of flexible ligands to proteins: parallel applications of AutoDock 2.4. *J. Comput.-Aided Mol. Des.* **1996**, *10*, 293–304.
- Goodsell, D. S.; Olson, A. J. Automated docking of substrates to proteins by simulated annealing. *Proteins* **1990**, *8*, 195–202.
- Weiner, S. J.; Kollman, P. A.; Case, D. A.; Singh, U. C.; Ghio, C.; Alagona, G.; Profeta, S., Jr.; Weiner, P. A new force field for molecular mechanical simulation of nucleic acids and proteins. *J. Am. Chem. Soc.* **1984**, *106*, 765–784.
- Besler, B. H.; Merz, K. M., Jr.; Kollman, P. A. Atomic charges derived from semiempirical methods. *J. Comput. Chem.* **1990**, *11*, 431–439.
- Hopfinger, A. J.; Malhotra, D.; Battershell, R. D.; Ho, A. W.; Chen, J. A. Conformational behavior and thermodynamic properties of phenothrin analogue insecticides. *Pestic. Sci.* **1984**, *9*, 631–641.
- Schulze-Gahmen, U.; Brandsen, J.; Jones, H. D.; Morgan, D. O.; Meijer, L.; Vesely, J.; Kim, S. H. Multiple modes of ligand recognition: crystal structures of cyclin-dependent protein kinase 2 in complex with ATP and two inhibitors, olomoucine and isopentenyladenine. *Proteins* **1995**, *22*, 378–391.
- Mohammadi, M.; Froum, S.; Hamby, J. M.; Schroeder, M. C.; Panek, R. L.; Lu, G. H.; Eliseenkova, A. V.; Green, D.; Schlesinger, J.; Hubbard, S. R. Crystal structure of an angiogenesis inhibitor bound to the FGF receptor tyrosine kinase domain. *EMBO J.* **1998**, *17*, 5896–5904.
- Trumpp-Kallmeyer, S.; Rubin, J. R.; Humblet, C.; Hamby, J. M.; Showalter, H. D. H. Development of a binding model to protein tyrosine kinases for substituted pyrido[2,3-d]pyrimidine inhibitors. *J. Med. Chem.* **1998**, *41*, 1752–1763.
- Brooks, B. R.; Brucoleri, R. E.; Olafson, B. D.; States, D. J.; Swaminathan, S.; Karplus, M. CHARMM: a program for macromolecular energy, minimization, and dynamics calculations. *J. Comput. Chem.* **1983**, *4*, 187–217.
- Frisch, M. J.; Trucks, G. W.; Schlegel, H. B.; Gill, P. M. W.; Johnson, B. G.; Robb, M. A.; Cheeseman, J. R.; Keith, T.; Petersson, G. A.; Montgomery, J. A.; Raghavachari, K.; Al-

Laham, M. A.; Zakrzewski, V. G.; Ortiz, J. V.; Foresman, J. B.; Cioslowski, J.; Stefanov, B. B.; Nanayakkara, A.; Challacombe, M.; Peng, C. Y.; Ayala, P. Y.; Chen, W.; Wong, M. W.; Andres, J. L.; Replogle, E. S.; Gomperts, R.; Martin, R. L.; Fox, D. J.; Binkley, J. S.; Defrees, D. J.; Baker, J.; Stewart, J. P.; Head-Gordon, M.; Gonzalez, C.; Pople, J. A. *Gaussian 94*, revision 94.D2; Gaussian, Inc.: Pittsburgh, PA, 1995.

- (38) Accelrys Inc., Scranton Rd., San Diego, CA, 2001.
- (39) Jorgensen, W. L.; Madura, J. D. Temperature and size dependence for Monte Carlo simulations of TIP4P water. *Mol. Phys.* **1985**, *56*, 1381–1392.

JM0201130